iScience

CellPress
OPEN ACCESS

Article

Early prediction of acute pancreatitis with acute kidney injury using abdominal contrast-enhanced CT features

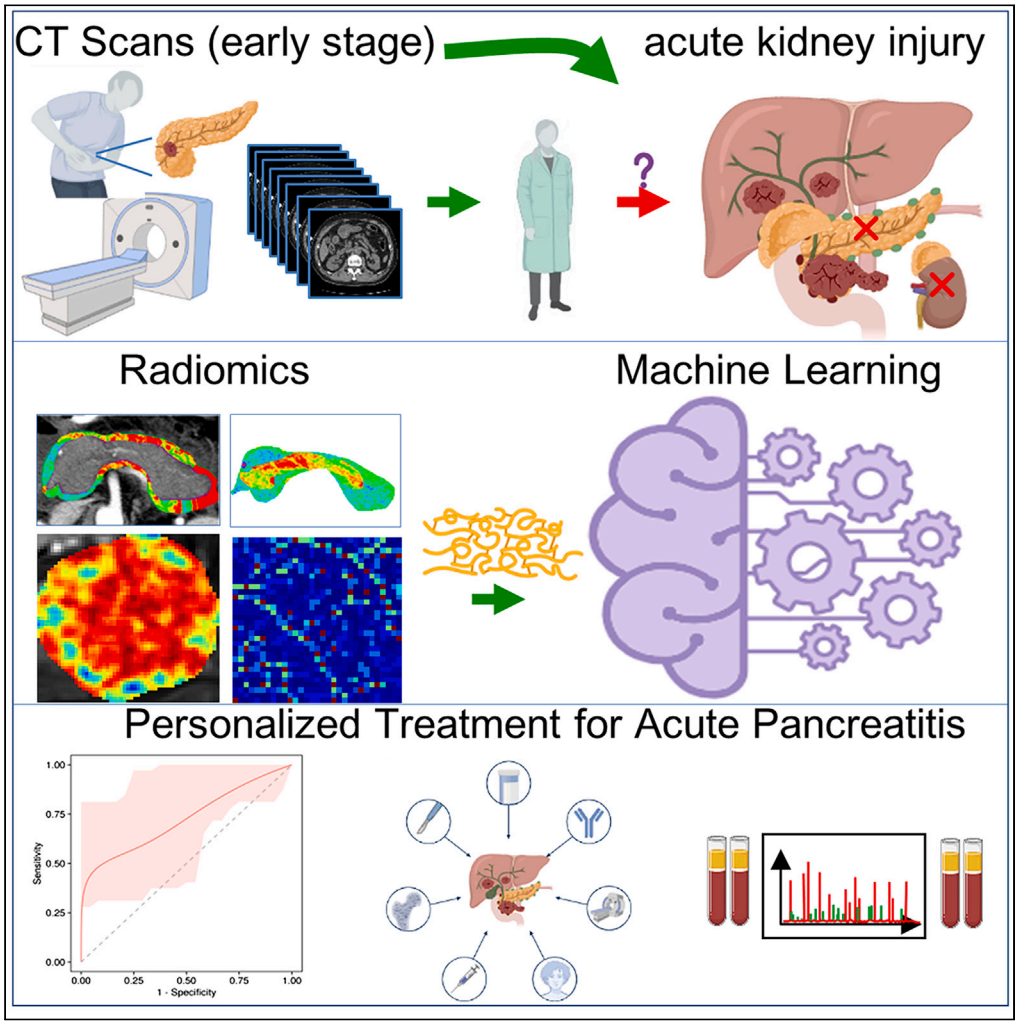

Lei Yuan, Mengyao Ji, Shanshan Wang, ..., Cheng Lu, Lei Shen, Jun Xu

shenlei818@whu.edu.cn (L.S.)
xujung@whu.edu.cn (J.X.)

Highlights

AI can early screen high-risk acute pancreatitis with acute kidney injury patients

The XGBM could early predict the occurrence of acute pancreatitis with acute kidney injury

This XGBM provides additional insights beyond laboratory tests alone for acute pancreatitis

Yuan et al., iScience 27, 111058
October 18, 2024 © 2024 The Author(s). Published by Elsevier Inc.
https://doi.org/10.1016/j.isci.2024.111058

iScience

CellPress
OPEN ACCESS

Article

Early prediction of acute pancreatitis with acute kidney injury using abdominal contrast-enhanced CT features

Lei Yuan,[1,2,3,6,8] Mengyao Ji,[4,6,8] Shanshan Wang,[4,6,8] Xuefang Lu,[5] Yong Li,[5] Pingxiao Huang,[5] Cheng Lu,[7] Lei Shen,[4,6,*] and Jun Xu[1,3,9,*]

SUMMARY

Early prediction of acute pancreatitis (AP) with acute kidney injury (AKI) using abdominal contrast-enhanced CT could effectively reduce the mortality and the economic burden on patients and society. However, this challenge is limited by the imaging manifestations of early-stage AP that are not clearly visible to the naked eye. To address this, we developed a machine learning model using imperceptible variations in the structural changes of pancreas and peripancreatic region, extracted by radiomics and artificial intelligence technology, to screen and stratify the high-risk AP patients at the early stage of AP. The results demonstrate that the machine learning model could screen the high-risk AP with AKI patients with an area under the curve (AUC) of 0.82 for the external cohort, superior to the human radiologists. This finding confirms the significant potential of machine learning in the screening of acute pancreatitis and contributes to personalized treatment and management for AP patients.

INTRODUCTION

Acute pancreatitis (AP), an inflammatory process affecting the pancreas, is the third most frequent gastrointestinal cause of hospital admissions in the United States.[1] Approximately, AP results in 300,000 hospital admissions annually, with associated costs of about $2.6 billion.[1,2] The incidence of AP is increasing and is estimated between 4.9 and 73.4 cases per 100,000 people, worldwide.[3,4] About 20% of AP patients will develop moderate severe acute pancreatitis (MSAP) or severe acute pancreatitis (SAP), and the mortality rate can reach 13%–35%.[5] Till now, various severity grading systems have been reported to predict the severity of AP. For instance, Ranson's criteria,[6] the Acute Physiology and Chronic Health Examination (APACHE) II[7] score, the bedside index for severity in acute pancreatitis (BISAP),[8] etc. Additionally, severity scales have also been devised based on computed tomography (CT) scan findings. For example, Balthazar score,[9] CT severity index (CTSI),[10] and other more recent research such as the modified CT severity index.[11] Both MSAP and SAP patients experience significant multi-organ failure (respiratory, cardiovascular, and kidney) as a prominent feature throughout the progression of the disease. Acute kidney injury (AKI) refers to an abrupt decrease in kidney function, resulting in the retention of urea and other nitrogenous waste products and in the dysregulation of extracellular volume and electrolytes. AKI is also a common and important complication of AP, and nearly 20% of ICU patients with AP developed AKI, leading to a high mortality of exceeding 60%.[12] As such, timely diagnosis and early prediction of the occurrence of AKI in AP (AP-AKI) patients is very important and urgent. However, few studies focus on early and accurate diagnosis of AKI in AP patients. To date, however, no comprehensive studies have evaluated the performance of contrast-enhanced CT features to predict AKI in AP, aiming to provide precise management of AP.

Although the imaging manifestations are not clearly visible in the early phase of acute pancreatitis,[13] there are still imperceptible variations in the structural changes within the pancreatic and/or peripancreatic/extrapancreatic tissue among patients with different levels of severity. These subtle differences can potentially be detected and quantified through the use of radiomics features, which refer to advanced imaging analysis techniques that extract a wide range of quantitative data by artificial intelligence (AI). By leveraging radiomics features, it becomes possible to uncover subtle nuances in the tissue changes associated with varying degrees of AP severity, thereby aiding in the accurate diagnosis and prognosis assessment of patients. Till now, artificial intelligence and machine learning technology have

[1]School of Automation, Nanjing University of Information Science and Technology, Nanjing, China
[2]Department of Information Center, Wuhan University Renmin Hospital, Wuhan, Hubei, China
[3]Jiangsu Key Laboratory of Big Data Analysis Technique, School of Automation, Nanjing University of Information Science and Technology, Nanjing, China
[4]Department of Gastroenterology, Wuhan University Renmin Hospital, Wuhan, Hubei, China
[5]Department of Radiology, Wuhan University Renmin Hospital, Wuhan, Hubei, China
[6]Key Laboratory of Hubei Province for Digestive System Disease, Wuhan University Renmin Hospital, Wuhan, Hubei, China
[7]Department of Radiology, Guangdong Provincial People's Hospital, Guangzhou, China
[8]These authors contributed equally
[9]Lead contact
*Correspondence: shenlei818@whu.edu.cn (L.S.), xujung@whu.edu.cn (J.X.)
https://doi.org/10.1016/j.isci.2024.111058

This is an open access article under the CC BY-NC license (http://creativecommons.org/licenses/by-nc/4.0/).

Table 1. Baseline patient characteristics

variables	sub variables	Total (*n* = 672)	D1 (*n* = 289)	D2 (*n* = 158)	D3(*n* = 126)	D4(*n* = 99)	P
gender, n(%)	male	359(53.4)	158(54.6)	107(58.7)	52(41.2)	42(42.4)	0.843
	female	131(46.6)	131(45.4)	51(41.3)	74(58.8)	57(57.6)	
age, (years)	–	48.6 ± 9.5	48.3 ± 5.2	48.9 ± 7.5	48.7 ± 8.9	49.5 ± 6.7	0.655
BMI, kg/m^2, n(%)	<30	272(40.5)	128(44.3)	63(39.8)	40(40.0)	41(31.7)	0.286
	≥30	400(59.5)	161(55.6)	95(60.2)	86(40.0)	58(68.3)	
Alcohol, n(%)	yes	382(56.8)	182(62.9)	96(60.7)	61(48.4)	43(43.5)	0.162
	no	290(43.2)	107(37.1)	62(39.3)	65(51.6)	56(56.5)	
Comorbid disease, n(%)	yes	436(64.8)	196(67.8)	89(56.3)	109(86.5)	42(42.4)	0.216
	no	236(35.2)	93(32.2)	69(43.7)	17(13.5)	57(57.6)	
Etiology, n(%)	biliary	315(46.8)	137(46.0)	77(48.7)	57(45.2)	44(44.4)	0.201
	alcoholic	179(26.6)	72(24.9)	46(29.1)	30(23.8)	31(31.3)	
	hyperlipidemia	99(14.7)	52(17.9)	26(16.4)	14(11.1)	7(7.1)	
	traumatic	65(9.6)	23(8.0)	6(3.8)	22(17.4)	14(14.1)	
	others	14(2.3)	5(1.7)	3(1.9)	3(2.4)	3(3.0)	
Type of AP, n(%)	interstitial edematous AP	644(95.8)	276(95.5)	150(94.9)	121(96.0)	97(97.9)	0.670
	necrotizing AP	28(4.2)	13(4.5)	8(5.1)	5(4.0)	2(2.1)	
AP-AKI, n(%)	yes	138(20.5)	58(20.2)	35(22.1)	27(21.4)	18(18.2)	0.164
	no	534(79.5)	231(14.8)	123(77.9)	99(78.6)	81(71.8)	

BMI: Body Mass Index, AP: acute pancreatitis, AP-AKI: acute pancreatitis with acute kidney injury. *p* values were derived from the $\chi 2$ test or Fisher exact test between D1, D2, D3 and D4.

made significant progress in medicine in recent years and has the potential to transform medicine.[14–17] Image digitization, offering insight into the heterogeneity of lesions that are unobservable with the naked eye, have made radiomics translate digital images into high-dimensional feature spaces, emerging as one of the most popular areas in health care.[18] Quantitative radiomics features, extracted by AI, could provide more subtle image-based attributes linked to tumor phenotypes and prognosis, beyond the naked eye and human subjective cognition.

As such, the purpose of this study was to use AI machine learning technology and abdominal contrast-enhanced CT quantitative features to construct predictive models derived from within and around the pancreatic lesions to early identify the AKI in AP patients, thereby achieving the potential of precision medicine in acute pancreatitis patients, as well as reducing morbidity and mortality.

RESULTS

Basic characteristics

A total of 672 patients diagnosed with acute pancreatitis were included in this study. The demographic characteristics of these patients are documented in Table 1. Among the AP patients, the majority (53.4%) was male, and the median age was 48.6 ± 9.5 years. Furthermore, it was observed that nearly 60% (400/672) of the patients had a body mass index (BMI) greater than 30 kg/m^2, indicating obesity. At the end of the follow-up period, around 20.5% (138/672) of the AP patients experienced acute pancreatitis with acute kidney injury.

Representative features

A total of 1,936 radiomics features were extracted from the abdominal contrast-enhanced CT; Table S1 referred to a more comprehensive radiomics feature list. Twelve radiomics features with nonzero coefficients were selected after feature selection by LASSO, as shown in Figure S1. After conducting univariable and multivariable logistic regression analysis, a total of 6 representative radiomics features were carefully identified, demonstrating their potential significance and informative in predicting the outcome AP-AKI, shown in Table 2. The top 6 discriminative radiomics features identified within the training cohort include wavelet decomposition of pancreatic and peripancreatic raidomics features. The pancreatic region radiomics features include the wavelet transformation result of the low-low-high (LHL) subband of the gray level variance (GLV) of the gray level dependence matrix (GLDM) feature (PA_WV_LHL_GLDM_GLV), the wavelet transformation result of the low-low-low (LLL) subband of the complexity of neighboring gray tone difference matrix (NGTDM) feature (PA_WV_LLL_NGTDM_Complexity), the wavelet transformation result of the low-high-high (LHH) subband of the size-zone non-uniformity (SZN) of gray level size zone matrix (GLSZM) feature (PA_WV_LHH_GLSZM_SZN) and the wavelet transformation result of the low-high-low (LHL) subband of the run variance (RV) of gray level run length matrix (GLRLM) feature (PA_WV_LHL_GLRLM_RV). The peripancreatic radiomics features include the wavelet transformation result of the low-high-low (LHL) subband of the SZN of GLSZM (EP_WV_LHH_GLSZM_SZN) and the wavelet transformation

Table 2. Univariable and multivariable logistic regression analysis of variables on D1

	univariate analysis		multivariate analysis	
variables	OR (95%CI)	P[a]	OR (95%CI)	P[b]
PA_WV_LHL_GLDM_GLV	6.18 (1.85,20.57)	0.003	5.69 (1.88,17.14)	0.002
PA_WV_LLL_NGTDM_Complexity	1.93 (1.17,3.16)	0.009	1.82 (1.15,2.87)	0.010
PA_WV_LHH_GLSZM_SZN	3.03 (1.22,7.46)	0.016	2.96 (1.20,7.27)	0.018
PA_WV_LLH_GLSZM_GLV	2.02(1.04,3.89)	0.036	–	–
PA_WV_LHL_GLRLM_RV	2.68(1.12,6.38)	0.026	2.49(1.10,5.58)	0.027
PA_WV_HLL_GLCM_DE	1.68(0.88,3.17)	0.111	–	–
PA_ WV_LHL_GLCM_DV	2.62(0.86,8.01)	0.091	–	–
PA_WV_LHL_first_order_uniformity	1.26(0.93,1.69)	0.127	–	–
EP_WV_LLL_GLSZM_ZV	3.22(0.56,18.50)	0.190	–	–
EP_WV_LHH_GLSZM_SZN	2.82(1.17,6.75)	0.020	2.52(1.14,5.56)	0.022
EP_WV_LLH_GLRLM_LRE	3.68(1.40,9.63)	0.008	3.60(1.37,9.41)	0.009
EP_WV_LHL_NGTDM_Contrast	1.46(0.89,2.38)	0.132	–	–

Note: PA: pancreatic region; EP: peripancreatic region; GLDM: Gray Level Dependence Matrix; NGTDM: Neighboring Gray Tone Difference Matrix; GLCM: Gray Level Co-occurrence Matrix; GLV: Gray Level Variance; GLSZM: Gray Level Size Zone Matrix; SZN: Size-Zone Non-Uniformity; GLRLM: Gray Level Run Length Matrix; RV: Run Variance; ZV: Zone Variance; LRE: Long Run Emphasis; SZN: Size-Zone Non-Uniformity; DV: Difference Variance; DE: Difference Entropy. **P[a] and P[b]** were derived from the univariate analysis and multivariate analysis, respectively.

result of the low-low-high (LLH) subband of the Long Run Emphasis (LRE) of GLRLM (EP_WV_LLH_GLRLM_LRE). Namely, these 6 radiomics features were statistically significantly associated with AP-AKI, independently.

The original abdominal contrast-enhanced CT images (Figures 1A and 1E), along with accompanying pancreatic parenchyma contours (Figures 1B and 1F), pancreatic feature maps and peripancreatic feature maps, were shown in Figure 1, representing AP-AKI and non AP-AKI groups from the first column to the fourth column. For the AP-AKI group, the overexpression of texture features in pancreatic and peripancreatic regions were observed, as shown in Figures 1C and 1D. Comparatively, the expression of radiomics texture features in pancreatic and peripancreatic regions was much lower for the low-risk group, as shown in Figures 1G and 1H.

Radiomics model performance

The XGBoost model (denoted by XGBM) was constructed using the 6 top discriminative radiomics features as aforementioned. The XGBM yield an area under the curve (AUC) of 0.90 (95% confidence interval [CI]: 0.78, 0.99) on D1, seen in Table S2 and Figure S2. As depicted in Figure 2A, the XGBM yield AUCs of 0.86 (95% CI: 0.80, 0.96) and 0.82 (95% CI: 0.79, 0.98) for identifying AP-AKI in D2 and D3, respectively. It was observed that the model predicted probability of AP-AKI showed excellent performance and closely matched the actual AP-AKI probability for all the groups under consideration (Figures 2B and S3), excluding some extreme points caused by false positive or false negative samples. The Brier scores of 0.06 and 0.08 were observed for D2 and D3, respectively.

Radiologists vs. XGBM

The radiologists' discrimination on D2 and D3 to early predict AP-AKI was shown in Figures 2C and 2D. Human reader1 achieved AUCs of 0.62 and 0.48 in D2 and D3, respectively, with corresponding Brier scores of 0.24 and 0.32, respectively. Meanwhile, human reader 2 obtained AUCs of 0.56 and 0.51, with corresponding Brief scores of 0.18 and 0.29, respectively. The human readers' calibrations on D2 and D3 were illustrated in Figures 2E and 2F, respectively.

Furthermore, a statistically significant positive correlation was revealed between the radiomics image classifier and the occurrence of AP-AKI (odds ratio [OR]: 16.42, 95%CI 2.23, 120.86, $p = 0.006$) on D2, as well as on D3 (OR: 13.68, 95%CI 1.92, 97.39, $p = 0.009$). While, for reader 1, no significant associations were observed on either D2 ($p = 0.320$) or D3 ($p = 0.261$). Similarly, for reader 2, a statistically significantly positive association was observed on D2 (OR: 1.83, 95%CI 1.42, 8.22, $p = 0.006$) but not on D3 ($p = 0.169$). Notable, the likelihood of occurrence of AP-AKI observed by the radiomics model was approximately 15 times and 7 times higher than that of human readers (OR: 16.42 vs. 1.93 and OR: 16.42 vs. 1.85) and APACHE II (OR: 16.42 vs. 2.36), as indicated in Table 3.

Association between XGBM and serum CRP

For D2, the radiomics classifier accurately predicted that 31 out of 158 AP patients as positive; out of these 31 XGBM-positive patients, 28 out of 31 XGBM-positive patients developed AP-AKI. In contrast, 7 out of 127 XGBM-negative patients developed AP-AKI, correspondingly. Comparatively, XGBM-positive patients' likelihood was over 16 times higher than that of XGBM-negative patients. Furthermore, our study

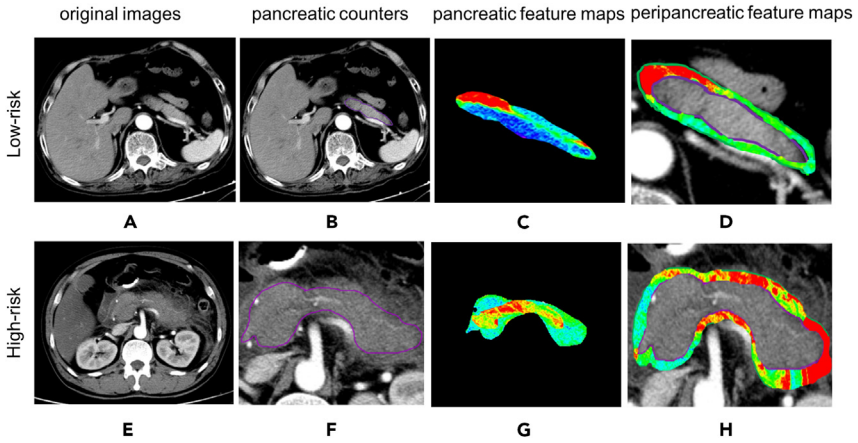

Figure 1. Pancreatic and peripancreatic radiomics features expression of Abdominal contrast-enhanced CT images for high and low-risk acute pancreatits with AKI

(A–F) Abdominal contrast-enhanced CT images analysis for acute pancreatitis patients with AKI (A), and without AKI (E). The original CT images (A and E) with accompanying region of pancreas counters (B, and F).Scale bar: 1mm. And corresponding feature maps (C, and G) were overlaid onto the counters. The last column (D, and F) showed the feature maps of peripancreatic region of (B) and (F). Scale bar: 50μm.

revealed that an overexpression of serum C-reactive protein (CRP) level was observed in 83.9% (26 out of 31) of XGBM-positive patients, compared to only 3.8% (5 out of 131) in the XGBM-negative group ($p < 0.001$), as shown in Figure 3A. Additionally, statistically significant differences were observed on D3 ($p < 0.001$) and D4 ($p < 0.001$), as illustrated in Figures 3B and 3C, respectively.

External validation and risk stratification

A total of 99 AP patients were enrolled in the external validation. Among these patients, the majority (61.3%) were male. The median age was 48 years. At the end of the follow-up, about 20% of the AP patients developed AP-AKI. The AUC of the XGBM was 0.81 (95% CI: 0.73, 0.89), along with corresponding Brier score of 0.09 (95% CI: 0.06, 0.12), as shown in Figures S4 and S5. Besides, the AP patients were stratified into high-risk and low-risk groups by utilizing the output generated by the XGBM model (cutoff value: 0.52). Additionally, the PR curves were shown in Figure S6.

DISCUSSION

AP is one of the most common diseases of the gastrointestinal tract, leading to tremendous emotional, physical, and financial human burden.[19] Worldwide, recent studies show the incidence of AP varies between 4.9 and 73.4 cases per 100,100 and continuously increasing, from 40 per 100,100 in 1998 to 70 per 100,000 in 2002. Acute kidney injury is a frequently occurring complication in patients with acute pancreatitis. Research has shown that AKI significantly increases the mortality rate in AP patients. Consequently, it is crucial to develop strategies for early prediction of the likelihood of AKI development in individuals diagnosed with acute pancreatitis. By accurately identifying patients at risk of developing AKI, prompt medical interventions and appropriate management strategies can be implemented, thus potentially reducing the mortality rate associated with this disease. However, the current diagnostic methods for AKI, urine output, and serum creatinine, have certain limitations due to their inherent measurement inaccuracy and delayed response to changes in kidney function. Fortunately, utilizing imaging techniques can provide a more precise analysis, and assessing functional parameters can help identify early tissue damage.

The main contributions of this study can be summarized as follows. (1) We developed and validated a radiomics machine learning model to predict the likelihood of AP-AKI, aiming to improve patient outcomes and reduce the overall burden on healthcare resources. (2) A preliminary study regarding XGBM outputs and serum CRP expressions association was analyzed. The XGBM yields excellent discrimination for the internal validation and independent external validation cohorts, with AUCs of 0.86, 0.82, and 0.81, respectively. In terms of model calibration, the Brier scores were 0.06, 0.08, and 0.09 for D2, D3, and D4, respectively. This indicated the XGBM's accuracy and stability in predicting the likelihood of APAKI. Additionally, we could easily stratify the diagnosed AP patients into different prognosis groups based on the radiomics model outputs. We could imagine with the help of this radiomics image classifier, risk assessment could be routinely performed to stratify AP patients into high-risk and low-risk categories to assist triage through contrast-enhanced computed tomography, such as admission to intensive care, as well as the individual therapeutic process.

The field of radiomics has experienced significant growth and advancement over the past few years. Radiomics refers to the extraction of quantitative features in a highly efficient and automated manner from radiographic images. The extraction and analysis of radiomics features provide valuable insights into tumor heterogeneity, treatment response, prognosis, and overall patient management. Furthermore, radiomics has the potential to identify subtle patterns and biomarkers that are not perceivable to the human eye, enabling earlier detection and more accurate diagnosis of diseases. In this study, we extracted a varying range of radiomics quantitative characteristics from radiographic images

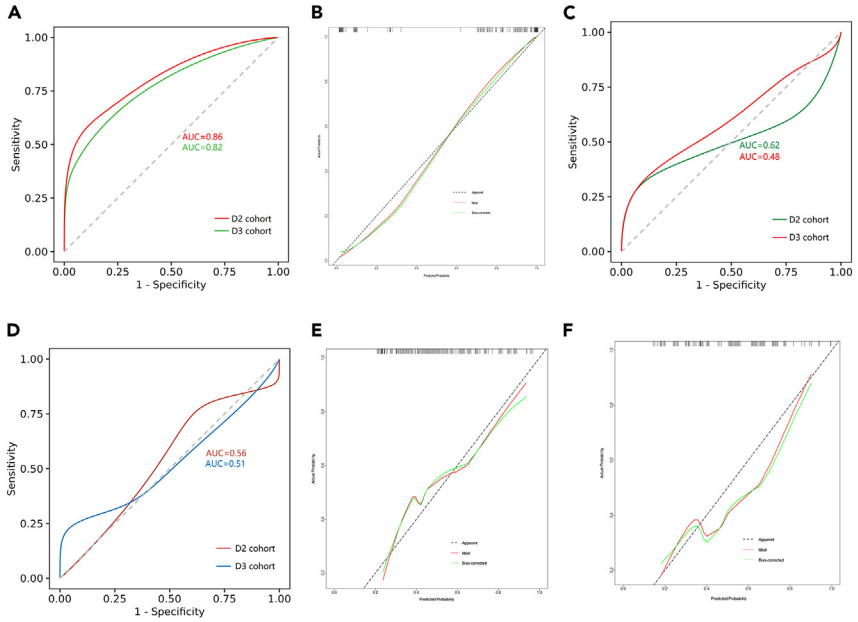

Figure 2. XGBM performance evaluations for predicting AP-AKI

(A) XGBM performance for D2 and D3, respectively.

(B) Validity of the XGBM predictive performance in estimating the risk of AP-AKI on D2.

(C) ROC curve for predicting AP-AIK by human reader1 on D2.

(D) ROC for predicting AP-AIK by human reader2 on D3.

(E) Validity of the human reader 1's predictive performance in estimating the risk of AP-AKI on D2.

(F) Validity of the human reader 2's predictive performance in estimating the risk of AP-AKI on D3.

and constructed a machine-learning radiomics model to predict the likelihood of AP-AKI. This designation could extract radiomics features in pancreatic along with peripancreatic tissues quantitatively and precisely. The results revealed that the wavelet transformation result of pancreatic and peripancreatic radiomics texture features beyond human eyes were closely linked to the higher risk of AP-AKI. The XGBM showed a strong positive association with AP-AKI (OR: 16.42, 95% CI: 2.23, 120.86) on D2. Additionally, the XGBM was proved to be statistically linked with the likelihood of AP-AKI on D3 (OR: 13.68, 95% CI: 1.92, 97.39), respectively. Furthermore, the radiomics model demonstrated a significantly higher predictive value for the occurrence of AP-AKI compared to both human readers (OR: 16.42 vs. 1.93 and OR: 16.42 vs. 1.85) and APACHE II (OR: 16.42 vs. 2.36).

Besides, we also inspected the discrimination difference between radiologists and XGBM for predicting the probability occurrence of AP-AKI. The univariate logistic regression analysis revealed that the human-based AP-AKI estimation scores were not statistically significant for AP-AKI prediction on D2 ($p = 0.320$) or D3 ($p = 0.261$) for human reader 1. Meanwhile, the human-based estimation scores of reader2 were strongly positively associated with the occurrence of AP-AKI on D2 ($p = 0.026$); while no statistical association was observed on D3 ($p = 0.169$). Comparatively, statistical associations were observed between XGAPI and the occurrence of AP-AKI on D2 ($p = 0.006$) and D3 ($p = 0.009$). This could be interpreted by the limitations and biases inherent in human visual perception, as radiologists routinely assess the severity of pancreatitis by observing the morphological changes in the pancreas. However, in the early stage of AP, the morphological changes of the pancreas are not readily obvious on CT images, resulting in the underestimation of the severity of acute pancreatitis. Furthermore, the clearly defined

Table 3. Univariable logistic regression analysis conducted on D2 and D3

	univariate analysis (D2)		univariate analysis (D3)	
variables	OR (95%CI)	P	OR (95%CI)	P
XGBM	16.42 (2.23,120.86)	0.006	13.68 (1.92,97.39)	0.009
Reader1 score	1.93 (0.52,7.05)	0.320	1.37(0.79,2.36)	0.261
Reader2 score	1.85 (1.07,3.17)	0.026	1.64 (0.81,3.31)	0. 169
APACHE II	2.36 (1.02,2.63)	0.041	2.09(0.91,4.75)	0. 079

XGBM: radiomics image classifier for predicting acute pancreatitis with acute kidney injury using XGBoost algorithm; APACHE II: Acute Physiology and Chronic Health Examination II. *p* values were derived from the univariate analysis on D2 and D3.

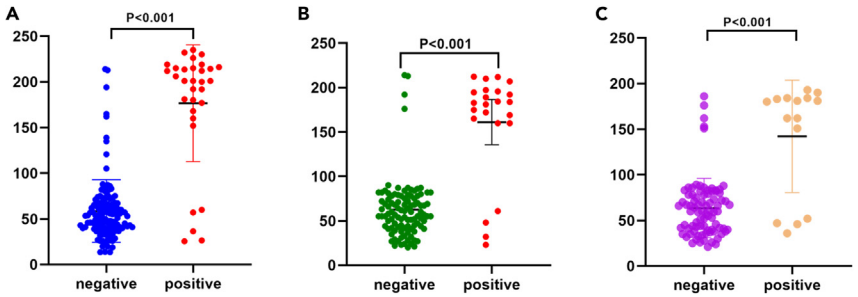

Figure 3. Serum CRP levels for different XGBM risk groups

(A–C) Serum CRP level distributions of XGBM-positive and XGBM-negative patients on D2, $p < 0.001$ (A), D3, $p < 0.001$ (B), and D4, $p < 0.001$ (C). XGBM: the XGBoost model for predicting AP-AKI; serum CRP: serum C-reactive protein. Data are means±standard deviations. $p < 0.05$ denotes statistical significance. An unpaired t test was used to compare the expression of serum CRP level between XGBM-positive and XGBM-negative groups.

criteria were lacking in terms of predicting the occurrence of AP-AKI in the early stage of AP. As such, the underestimated decision might be made by the radiologists according to the individual observations on pancreatic and/or peripancreatic morphological profiles, such as focal or diffuse enlargement of the pancreas, inflammatory changes in peripancreatic fat, pancreatic or peripancreatic fluid collection or other profiles subjectively. Conversely, the radiomics could extract subtle quantitative information in terms of pancreatic/peripancreatic morphological changes, which cannot be detected by radiologists alone, objectively. Furthermore, our preliminary investigation has provided compelling evidence to support a strong correlation between the XGBM-positive and the overexpression of CRP in AP patients. Specifically, a statistically significant association was observed, with 83.9% of XGBM-positive acute pancreatitis patients exhibiting overexpression of serum CRP, compared to only 3.8% of XGBM-negative acute pancreatitis patients displayed similar overexpression ($p < 0.001$).

Our study identified six discriminative radiomic features, including PA_WV_LHL_GLDM_GLV, PA_WV_LLL_NGTDM_Complexity, PA_WV_LHH_GLSZM_SZN, PA_WV_LHL_GLRLM_RV, EP_WV_LHH_GLSZM_SZN, EP_WV_LLH_ GLRLM_ LRE, which were statistically significant linked with the occurrence of AP-AKI. Generally, in the early stage of AP, the manifestations are not obvious for radiologists, to assess the severity of AP by the morphological changes of the pancreas. However, radiomics could deeply uncover hidden information related to lesion heterogeneity or tissue morphological changes that are not discernible to the naked eye. For instance, the evidence revealed that in the early stages of symptom onset, there is an increase in blood flow in mild acute pancreatitis. Comparatively, patients with moderate and severe pancreatitis experience a progressive decrease in blood flow (tissue ischemia) and impaired perfusion to the pancreatic tissues.[20] From the findings, it is perceived that there is damage to the pancreatic parenchyma caused by disruptions in the microcirculation during the initial stages of the disease. These changes are not easily detectable through routine examinations. Our study demonstrated that radiomics can potentially provide valuable insights into the early-stage damage to the pancreatic parenchyma and peripancreatic region. By analyzing radiomic features, such as texture analysis and wavelet-based measurements, specific patterns and abnormalities indicative of pancreas tissue damage can be identified. These findings regarding radiomics are consistent with previous studies.[21–23] Notable, the optimal discriminative radoimic features associated with AP-AKI were all from the wavelet-based texture features (4 pancreatic features and 3 peripancreatic features). This could be interpreted by the mechanism of acute pancreatitis inflammation.

Inflammation of the pancreatic tissue undergoes a series of changes such as congestion, edema, and even necrosis, resulting in a significantly uneven texture of the pancreas and peripancreatic region. The inflammation process causes the pancreatic tissue to become swollen, congested with blood, and affected by cell death. These alterations not only disrupt the normal structure of the pancreas but also contribute to the development of necrotic (dead) tissue. Consequently, the texture of the pancreas becomes irregular, with areas of normal tissue interspersed with inflamed and necrotic regions. The peripancreatic region, which encompasses the pancreas, is further complicated by a combination of exudate and adipose tissue. Exudate refers to the fluid and cells that extravasate from blood vessels during inflammation. The presence of this fluid in conjunction with the fatty tissue surrounding the pancreas results in a significant variation in the average gray level of the peripancreatic area as captured by radiomics, but not discernible to the naked eye. Indeed, the SZN measures the variability in the sizes of zones (connected regions with the same gray level), providing insight into the texture's uniformity. The LHH subband of the wavelet transformation highlights texture features at a finer scale and can be crucial in identifying specific patterns or anomalies within regions of interest. Therefore, SZN values in the LHH subband could reflect differences in texture uniformity at multiple scales, capturing subtle variations in the gray-level size zone patterns. These features might indicate differences in tissue texture, which can be critical for distinguishing between benign and malignant conditions. This may be the main reason why the WV_LHH_GLSZM_SZN appears simultaneously in the feature sets of both the pancreas and peripancreatic regions. Additionally, this could be interpreted by the biological relationship. Biologically, the pancreas and peripancreatic regions are closely related anatomically and functionally. Pathological conditions affecting the pancreas often extend to the peripancreatic tissues. Therefore, a shared texture feature in these regions might reflect underlying physiological or pathological processes that affect both areas, simultaneously.

In conclusion, the radiomics features extracted from contrast-enhanced CT scans have the potential to capture hidden differences within the pancreatic parenchyma and peripancreatic region in AP patients, particularly during the early stages of the disease. Utilizing radiomics can provide clinicians with valuable insights into disease progression and facilitate more informed decision-making regarding AP patient

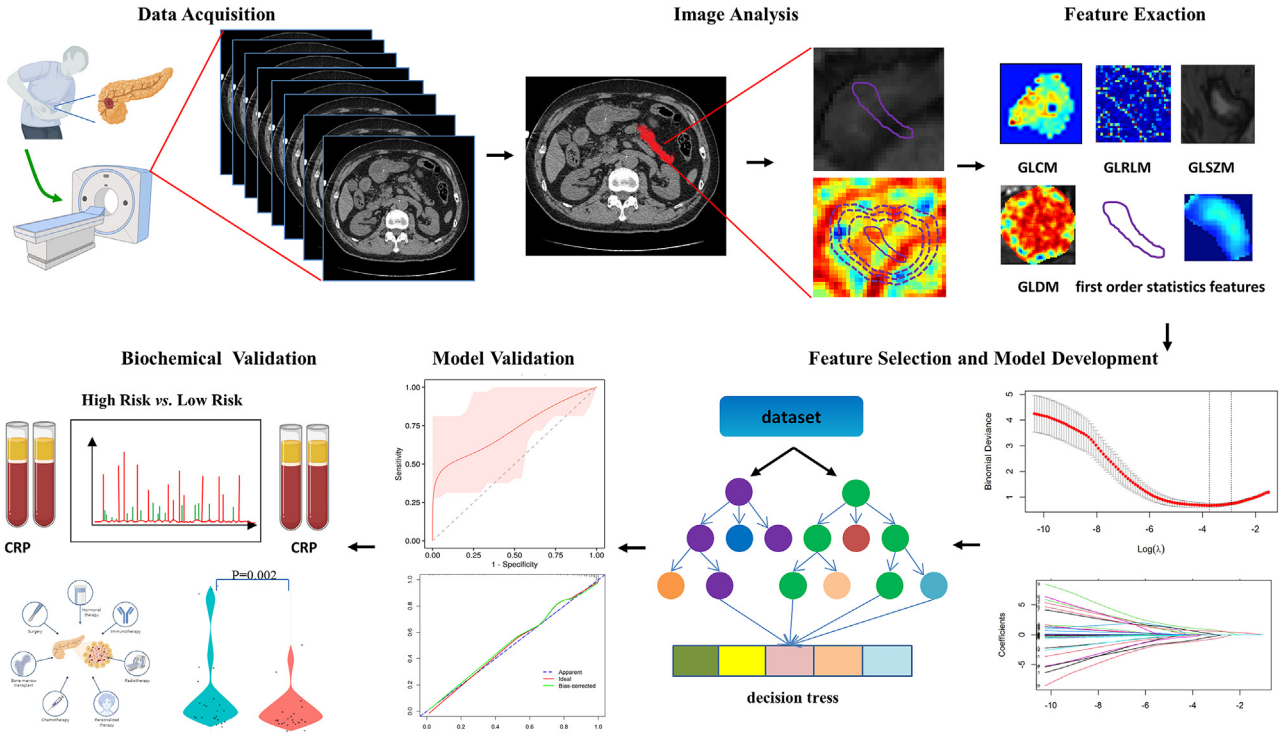

Figure 4. The overall pipeline for this study, consisting of data acquisition, image analysis, feature exaction, feature selection, model development, model validation, and biochemical validation

Scale bar: 2mm.

management. This approach may aid in identifying high-risk patients who require intensive care or early interventions, while also enabling the identification of low-risk patients who may be managed conservatively. Nevertheless, further research and validation studies are necessary to fully establish the clinical utility of this method.

Limitation of the study

We acknowledged, however, that our study has its limitations. Firstly, the XGBM model was initially developed using data primarily obtained from Chinese patients, and further validation in diverse racial groups is necessary before generalizing to AP patients. Secondly, this study was completely retrospective, requiring further prospective validation to confirm the model's performance. Finally, the pilot study in terms of the association between XGBM outputs and serum CRP may be limited by the small sample size.

RESOURCE AVAILABILITY

Lead contact

Further information and requests should be directed to the lead contact, JunXu (xujung@whu.edu.cn).

Materials availability

This study did not generate new unique reagents.

Data and code availability

- All data reported in this paper will be shared by the lead contact upon request.
- All original code has been deposited at github and is publicly available as of the date of publication.
- Any additional information required to reanalyze the data reported in this paper is available from the lead contact upon request.

ACKNOWLEDGMENTS

Special thanks to The Center for Computational Imaging and Personalized Diagnostics (CCIPD) and their team members in Emory University for their wonderful assistance with digital analysis support.

Funding: This work was supported by the National Key Research and Development Program of China (2023YFC3402800); The National Natural Science Foundation of China (81901817, 62171230, 62101365, 92159301, 91959207, 62301263, 62301265, 62302228, 82302291, 82302352); Hubei Provincial Key Laboratory Project (2021KFY051).

AUTHOR CONTRIBUTIONS

M.Y.J., L.S., and J.X. had the idea for and designed the study. L.Y. and W.S.S. contributed to writing the paper. Y.X.L., X.F.L., and L.Y. contributed to collect data. L.Y. contributed to the statistical analysis. All authors contributed to data acquisition, data analysis, or data interpretation, reviewed and approved the final version.

DECLARATION OF INTERESTS

The authors declare no competing interests.

STAR★METHODS

Detailed methods are provided in the online version of this paper and include the following:

- KEY RESOURCES TABLE
- EXPERIMENTAL MODEL AND STUDY PARTICIPANT DETAILS
  - Ethics statement
  - Study population
  - Inclusion and exclusion criteria
- METHOD DETAILS
  - Abdominal CT protocol
  - Serum C-reactive protein
  - Clinical outcome
  - Image analysis and feature exaction
  - Feature selection
  - Radiomicss model development, evaluation and risk stratification
  - Human reader studies
- QUANTIFICATION AND STATISTICAL ANALYSIS

SUPPLEMENTAL INFORMATION

Supplemental information can be found online at https://doi.org/10.1016/j.isci.2024.111058.

Received: May 14, 2024
Revised: July 19, 2024
Accepted: September 24, 2024
Published: September 27, 2024

REFERENCES

1. Jin, D.X., McNabb-Baltar, J.Y., Suleiman, S.L., Wu, B.U., Khorasani, R., Bollen, T.L., Banks, P.A., and Singh, V.K. (2017). Early Abdominal Imaging Remains Over-Utilized in Acute Pancreatitis. Dig. Dis. Sci. *62*, 2894–2899. https://doi.org/10.1007/s10620-017-4720-x.
2. Shyu, J.Y., Sainani, N.I., Sahni, V.A., Chick, J.F., Chauhan, N.R., Conwell, D.L., Clancy, T.E., Banks, P.A., and Silverman, S.G. (2014). Necrotizing Pancreatitis: Diagnosis, Imaging, and Intervention. Radiographics *34*, 1218–1239. https://doi.org/10.1148/rg.345130012.
3. Lombardo, I., and Dighe, M. (2014). Acute Pancreatitis: ACR Appropriateness Criteria Commentary. Ultrasound Q. *30*, 274–275. https://doi.org/10.1097/Ruq.0000000000000116.
4. Yadav, D., and Lowenfels, A.B. (2006). Trends in the epidemiology of the first attack of acute pancreatitis - A systematic review. Pancreas *33*, 323–330. https://doi.org/10.1097/01.mpa.0000236733.31617.52.
5. van Dijk, S.M., Hallensleben, N.D.L., van Santvoort, H.C., Fockens, P., van Goor, H., Bruno, M.J., and Besselink, M.G.; Dutch Pancreatitis Study Group (2017). Acute pancreatitis: recent advances through randomised trials. Gut *66*, 2024–2032. https://doi.org/10.1136/gutjnl-2016-313595.
6. Ranson, J.H.,R.K., Roses, D.F., Fink, S.D., Eng, K., and Spencer, F.C. (1974). Prognostic signs and the role of operative management in acute pancreatitis. Surgery, gynecology & obstetrics *139*, 69–81.
7. Knaus, W.A., Draper, E.A., Wagner, D.P., and Zimmerman, J.E. (1985). Apache-Ii - a Severity Of Disease Classification-System. Crit. Care Med. *13*, 818–829. https://doi.org/10.1097/00003246-198510000-00009.
8. Wu, B.U., Johannes, R.S., Sun, X., Tabak, Y., Conwell, D.L., and Banks, P.A. (2008). The early prediction of mortality in acute pancreatitis: a large population-based study. Gut *57*, 1698–1703. https://doi.org/10.1136/gut.2008.152702.
9. Balthazar, E.J., Ranson, J.H., Naidich, D.P., Megibow, A.J., Caccavale, R., and Cooper, M.M. (1985). Acute-Pancreatitis - Prognostic Value Of Ct. Radiology *156*, 767–772. https://doi.org/10.1148/radiology.156.3.4023241.
10. Balthazar, E.J., Robinson, D.L., Megibow, A.J., and Ranson, J.H. (1990). Acute-Pancreatitis - Value Of Ct In Establishing Prognosis. Radiology *174*, 331–336. https://doi.org/10.1148/radiology.174.2.2296641.
11. Mortele, K.J., Wiesner, W., Intriere, L., Shankar, S., Zou, K.H., Kalantari, B.N., Perez, A., vanSonnenberg, E., Ros, P.R., Banks, P.A., and Silverman, S.G. (2004). A modified CT severity index for evaluating acute pancreatitis: Improved correlation with patient outcome. AJR. Am. J. Roentgenol. *183*, 1261–1265. https://doi.org/10.2214/ajr.183.5.1831261.
12. Lin, H.Y., Lai, J.I., Lai, Y.C., Lin, P.C., Chang, S.C., and Tang, G.J. (2011). Acute renal failure in severe pancreatitis: A population-based study. Ups. J. Med. Sci. *116*, 155–159. https://doi.org/10.3109/03009734.2010.547636.
13. Tenner, S., Baillie, J., DeWitt, J., and Vege, S.S.; American College of Gastroenterology (2013). American College of Gastroenterology Guideline: Management of Acute Pancreatitis. Am. J. Gastroenterol. *108*, 1400–1416. https://doi.org/10.1038/ajg.2013.218.
14. Yuan, L., Ji, M., Wang, S., Wen, X., Huang, P., Shen, L., and Xu, J. (2022). Machine learning model identifies aggressive acute pancreatitis within 48 h of admission: a large retrospective study. BMC Med. Inf. Decis. Making *22*, 312. https://doi.org/10.1186/s12911-022-02066-3.
15. Yuan, L., Shen, L., Ji, M., Wen, X., Wang, S., Huang, P., Li, Y., and Xu, J. (2023). A New Risk Score to Predict Intensive Care Unit Admission for Patients with Acute

Pancreatitis 48 Hours After Admission: Multicenter Study. Dig. Dis. Sci. *68*, 2069–2079. https://doi.org/10.1007/s10620-022-07768-2.

16. Ding, R., Prasanna, P., Corredor, G., Barrera, C., Zens, P., Lu, C., Velu, P., Leo, P., Beig, N., Li, H., et al. (2022). Image analysis reveals molecularly distinct patterns of TILs in NSCLC associated with treatment outcome. npj Precis. Oncol. *6*, 33. https://doi.org/10.1038/S41698-022-00277-5.
17. Wang, X., Bera, K., Barrera, C., Zhou, Y., Lu, C., Vaidya, P., Fu, P., Yang, M., Schmid, R.A., Berezowska, S., et al. (2021). A prognostic and predictive computational pathology image signature for added benefit of adjuvant chemotherapy in early stage non-small-cell lung cancer. EBioMedicine *69*, 103481. https://doi.org/10.1016/J.Ebiom.2021.103481.
18. Bertsimas, D., and Wiberg, H. (2020). Machine Learning in Oncology: Methods, Applications, and Challenges. Jco Clin Cancer Info *4*, 885–894. https://doi.org/10.1200/Cci.20.00072.
19. Peery, A.F., Crockett, S.D., Murphy, C.C., Jensen, E.T., Kim, H.P., Egberg, M.D., Lund, J.L., Moon, A.M., Pate, V., Barnes, E.L., et al. (2022). Burden and Cost of Gastrointestinal, Liver, and Pancreatic Diseases in the United States: Update 2021. Gastroenterology *162*, 621–644. https://doi.org/10.1053/j.gastro.2021.10.017.
20. Kotan, R., Peto, K., Deak, A., Szentkereszty, Z., and Nemeth, N. (2022). Hemorheological and Microcirculatory Relations of Acute Pancreatitis. Metabolites *13*, 4. Artn 4. https://doi.org/10.3390/Metabo13010004.
21. Lin, Q., Ji, Y.F., Chen, Y., Sun, H., Yang, D.D., Chen, A.L., Chen, T.W., and Zhang, X.M. (2020). Radiomics model of contrast-enhanced MRI for early prediction of acute pancreatitis severity. J. Magn. Reson. Imag. *51*, 397–406. https://doi.org/10.1002/jmri.26798.
22. Zhao, Y., Wei, J., Xiao, B., Wang, L., Jiang, X., Zhu, Y., and He, W. (2023). Early prediction of acute pancreatitis severity based on changes in pancreatic and peripancreatic computed tomography radiomics nomogram. Quant. Imag. Med. Surg. *13*, 1927–1936. https://doi.org/10.21037/qims-22-821.
23. Mukherjee, S., Patra, A., Khasawneh, H., Korfiatis, P., Rajamohan, N., Suman, G., Majumder, S., Panda, A., Johnson, M.P., Larson, N.B., et al. (2022). Radiomics-based Machine-learning Models Can Detect Pancreatic Cancer on Prediagnostic Computed Tomography Scans at a Substantial Lead Time Before Clinical Diagnosis. Gastroenterology *163*, 1435–1446.e3. https://doi.org/10.1053/j.gastro.2022.06.066.
24. Isensee, F., Jaeger, P.F., Kohl, S.A.A., Petersen, J., and Maier-Hein, K.H. (2021). nnU-Net: a self-configuring method for deep learning-based biomedical image segmentation. Nat. Methods *18*, 203–211. https://doi.org/10.1038/s41592-020-01008-z.
25. Banks, P.A., Bollen, T.L., Dervenis, C., Gooszen, H.G., Johnson, C.D., Sarr, M.G., Tsiotos, G.G., and Vege, S.S.; Acute Pancreatitis Classification Working Group (2013). Classification of acute pancreatitis–2012: revision of the Atlanta classification and definitions by international consensus. Gut *62*, 102–111. https://doi.org/10.1136/gutjnl-2012-302779.
26. Chawla, N.V., Bowyer, K.W., Hall, L.O., and Kegelmeyer, W.P. (2002). SMOTE: Synthetic minority over-sampling technique. J. Artif. Intell. Res. *16*, 321–357. https://doi.org/10.1613/Jair.953.
27. Zhu, Y., Ji, M., Yuan, L., Yuan, J., and Shen, L. (2024). A risk prediction model for delayed bleeding after ESD for gastric precancerous lesions. Surg. Endosc. *38*, 3967–3975. https://doi.org/10.1007/s00464-024-10923-7.
28. Lankisch, P.G., Apte, M., and Banks, P.A. (2015). Acute pancreatitis. Lancet *386*, 85–96. https://doi.org/10.1016/S0140-6736(14)60649-8.
29. Dervenis, C., Beger, H.G., and Isenmann, R. (1999). Diagnosis, objective assessment of severity, and management of acute pancreatitis - Santorini Consensus Conference. Int. J. Pancreatol. *26*, 1–2.
30. Kidney, F.N., and Kidney, D. (2013). KDIGO 2012 Clinical Practice Guideline for the Evaluation and Management of Chronic Kidney Disease.
31. Mehta, R.L., Kellum, J.A., Shah, S.V., Molitoris, B.A., Ronco, C., Warnock, D.G., and Levin, A.; Acute Kidney Injury Network (2007). Acute Kidney Injury Network: report of an initiative to improve outcomes in acute kidney injury. Crit. Care *11*, R31. https://doi.org/10.1186/cc5713.
32. Bellomo, R., Ronco, C., Kellum, J.A., Mehta, R.L., and Palevsky, P.; Acute Dialysis Quality Initiative workgroup (2004). Acute renal failure - definition, outcome measures, animal models, fluid therapy and information technology needs: the Second International Consensus Conference of the Acute Dialysis Quality Initiative (ADQI) Group. Crit. Care *8*, R204–R212. https://doi.org/10.1186/cc2872.
33. Beer, J.C., Tustison, N.J., Cook, P.A., Davatzikos, C., Sheline, Y.I., Shinohara, R.T., and Linn, K.A.; Alzheimer's Disease Neuroimaging Initiative (2020). Longitudinal ComBat: A method for harmonizing longitudinal multi-scanner imaging data. Neuroimage *220*, 117129. https://doi.org/10.1016/j.neuroimage.2020.117129.
34. Yushkevich, P.A., Piven, J., Hazlett, H.C., Smith, R.G., Ho, S., Gee, J.C., and Gerig, G. (2006). User-guided 3D active contour segmentation of anatomical structures: significantly improved efficiency and reliability. Neuroimage *31*, 1116–1128. https://doi.org/10.1016/j.neuroimage.2006.01.015.
35. Xia, T.Y., Zhou, Z.H., Meng, X.P., Zha, J.H., Yu, Q., Wang, W.L., Song, Y., Wang, Y.C., Tang, T.Y., Xu, J., et al. (2023). Predicting Microvascular Invasion in Hepatocellular Carcinoma Using CT-based Radiomics Model. Radiology *307*, e222729. https://doi.org/10.1148/radiol.222729.
36. van Griethuysen, J.J.M., Fedorov, A., Parmar, C., Hosny, A., Aucoin, N., Narayan, V., Beets-Tan, R.G.H., Fillion-Robin, J.C., Pieper, S., and Aerts, H.J.W.L. (2017). Computational Radiomics System to Decode the Radiographic Phenotype. Cancer Res. *77*, e104–e107. https://doi.org/10.1158/0008-5472.CAN-17-0339.
37. Tang, X. (1998). Texture information in run-length matrices. IEEE Trans. Image Process. *7*, 1602–1609. https://doi.org/10.1109/83.725367.
38. Thibault, G., Fertil, B., Navarro, C., Pereira, S., Cau, P., Levy, N., Sequeira, J., and Mari, J.L. (2013). Shape and texture indexes - Application to cell nuclei classification. Int. J. Pattern Recogn. Artif. Intell. *27*, 1357002.
39. Tibshirani, R., Bien, J., Friedman, J., Hastie, T., Simon, N., Taylor, J., and Tibshirani, R.J. (2012). Strong rules for discarding predictors in lasso-type problems. J. R. Stat. Soc. Series B Stat. Methodol. *74*, 245–266. https://doi.org/10.1111/j.1467-9868.2011.01004.x.
40. Collins, G.S., Reitsma, J.B., Altman, D.G., and Moons, K.G.M. (2015). Transparent reporting of a multivariable prediction model for individual prognosis or diagnosis (TRIPOD): the TRIPOD statement. Br. Med. J. *350*, g7594. https://doi.org/10.1136/bmj.g7594.
41. Grau, J., Grosse, I., and Keilwagen, J. (2015). PRROC: computing and visualizing precision-recall and receiver operating characteristic curves in R. Bioinformatics *31*, 2595–2597. https://doi.org/10.1093/bioinformatics/btv153.
42. Manning, D.W., Edelstein, A.I., and Alvi, H.M. (2016). Risk Prediction Tools for Hip and Knee Arthroplasty. J. Am. Acad. Orthop. Surg. *24*, 19–27. https://doi.org/10.5435/JAAOS-D-15-00072.
43. Marsaglia, G., Tsang, W.W., and Wang, J. (2003). Evaluating Kolmogorov's Distribution. J. Stat. Software *8*.
44. Cohen, J. (1968). Weighted kappa: nominal scale agreement with provision for scaled disagreement or partial credit. Psychol. Bull. *70*, 213–220. https://doi.org/10.1037/h0026256.

STAR★METHODS

KEY RESOURCES TABLE

REAGENT or RESOURCE	SOURCE	IDENTIFIER
Software and algorithm		
nnU-Net	Isensee et al. (2021)[24]	https://doi.org/10.1038/s41592-020-01008-z
Python	Version 3.80	https://www.python.org/downloads/release/python-380
ITK-SNAP	Version 4.0.2	http://www.itksnap.org/pmwiki/pmwiki.php
R	Version 4.2.2	https://cran.r-project.org/src/base/R-4/
Prediction model (XGBM)	This study	Request from lead contact (xujung@whu.edu.cn)

EXPERIMENTAL MODEL AND STUDY PARTICIPANT DETAILS

Ethics statement

Our study was approved by the ethical committee of Renmin Hospital of Wuhan University (2021ks06169) and the Central Hospital of Wuhan, Tongji Medical College, Huazhong University of Science and Technology (202103199) and abided with the Declaration of Helsinki before using tissue samples for scientific research purposes only. The written informed consent was waived by the ethical committee for this retrospective study.

Study population

The pipeline of this study, including data acquisition, image analysis, feature extraction, feature selection, model development, model validation, and biochemical validation, is shown in Figure 4. First, AP patients with AKI were retrospectively enrolled in this study. The data used in this study were collected retrospectively from three independent institutions: Renmin Hospital of Wuhan University from January 6, 2016, to October 22, 2020, the Central Hospital of Wuhan, Tongji Medical College, and Suining Central Hospital between 2018 and 2019. It included 672 patients with 53.4% of male and the median age was 48.6 $\pm$ 9.5 years. The local institutional review board approved the study and waived the requirement for informed consent. Acute pancreatitis diagnosis was confirmed according to the revised Atlanta classification of acute pancreatitis in 2012.[25] The diagnosis of acute pancreatitis is defined by the presence of two of the following: (1) acute onset of persistent, severe, epigastric pain often radiating to the back; (2) elevation in serum lipase or amylase to three times or greater than the upper limit of normal; (3) characteristic findings of acute pancreatitis on imaging. This multicenter retrospective study contained four cohorts: an internal training cohort (D1 = 289), used for model development. 54.6% were male and the median age was 48.3 $\pm$ 5.2 years; an internal test cohort (D2 = 158), used for model validation with 58.7% were male and the median age was 48.9 $\pm$ 7.5 years; two external test cohorts (D3 = 126 and D4 = 99), used for assessing the model generalization. Among them, the proportion of males was 41.2% and 42.4% and the median age was 48.7 $\pm$ 8.9 and 49.5 $\pm$ 6.7 for D3 and D4, respectively. Before the data were used for model training, testing, and reader studies, all identifying information was removed from the data in this study. To handle unbalanced classification problems in the training data, the SMOTE algorithm[26] was utilized in this study as our previous work.[27] The R software with the 'DMwR package was used to generate minority class.

Inclusion and exclusion criteria

Inclusion criteria: (1) Patients who were admitted to the hospital and diagnosed with acute pancreatitis (AP) using the international consensus guidelines[28]; (2) Patients with complete clinical course record; (3) Patients underwent abdominal contrast-enhanced CT. Exclusion criteria: (1) Chronic pancreatitis patients with recurrent acute attacks; (2) Patients with incomplete clinical data; (3) Patients with a history of chronic renal failure; (4) AKI duo to other factors, such as sepsis, hypotension or shock, nephrotoxic medications, dehydration or volume depletion, pre-existing chronic kidney disease, etc. the inclusion and exclusion process was illustrated in Figure S7.

METHOD DETAILS

Abdominal CT protocol

CT images were obtained from the picture archiving and communication system (PACS), including non-contract and arterial, portal venous, and delayed phases post contrast. Enrolled patients at the three institutions had similar scan protocols: arterial phase scanning were initiated with 15–20 s delay after enhancement of the descending aorta to 100–120 HU; portal and delayed phase images were obtained at 70 and 180 s, respectively, after contrast injection. The imaging protocols are detailed in Data S1.

Serum C-reactive protein

After 48 h of the onset of symptoms, 5 mL venous blood was collected from the ulnar vein. The collected sample was then subjected to centrifugation at a speed of 1000×g for 20 min. The clear liquid was collected from the top layer and stored at a temperature of −20°C to maintain its stability and integrity for future analysis. The level of C-reactive protein (CRP) was determined by BNII protein analyzer (Siemens, Germany). Serum CRP was detected by colorimetric method, referring to >150 mg/L as the overexpression of CRP, as suggested by Dervenis C et al..[29]

Clinical outcome

The acute pancreatitis with acute kidney injury was defined as the primary clinical outcome of follow-up in this study. The diagnostic criteria of acute kidney injury were determined based on the guidelines of the Kidney Disease Improving Global Outcomes (KIDGO).[30] The KDIGO guidelines define AKI as follows: (1) Increase in serum creatinine by $\geq$ 0.3 mg/dL ($\geq$ 26.5 μmol/L) within 48 h or; (2) Increase in serum creatinine to $\geq$ 1.5 times baseline, which is known or presumed to have occurred within the prior seven days, or; (3) Urine volume <0.5 mL/kg/h for 6 h. The time frame for an absolute increase in serum creatinine of $\geq$ 0.3 mg/dL is retained from the acute kidney injury network (AKIN) definition[31] (48 h); while the time frame for a $\geq$ 50 percent increase in serum creatinine reverted to the 7 days originally included in the Acute Dialysis Quality Initiative (ADQI) RIFLE (Risk, Injury, Failure, Loss of kidney function, and End-stage kidney disease) criteria.[32] The follow-up period of patients began from the diagnosis of acute pancreatitis to the development of acute pancreatitis with kidney injury or the patient was cured and discharged.

Image analysis and feature exaction

The ComBat algorithm[33] was used to eliminate the batch effects in high-throughput data, removing the center-dependent impact of scanner parameter variations for radiomic characteristics between different institutions. Two abdominal radiologists (with >5 years' experience in the field of abdomen imaging) were employed to manually delineate the pancreas parenchyma without knowledge of the patient's clinical outcome, respectively. The disagreements were resolved with consensus. The region of interest (ROI) of the pancreatic parenchyma was delineated manually using ITK-SNAP software (version 4.0.0).[34] A 5-mm-wide band was automatically created by dilating the pancreatic parenchyma boundaries as the peripancreatic region, similar to our previous study.[35] Next, the nnu-Net algorithm,[24] an automatic segmentation method based on deep learning, was used to segment the pancreatic parenchyma, automatically (Data S2). Pyradiomics,[36] an open-source python package for the extraction of radiomics features from medical imaging, was employed to get the abdominal contrast-enhanced CT features. Three types of radiomics features were extracted, including fist-order statistics (N = 19), shape-based features (N = 27), textural features (N = 75) and wavelet-based feature (N = 752). And the textural features include gray level co-occurrence matrix features (GLCM), gray level run length matrix (GLRLM),[37] gray level size zone matrix (GLSZM) features,[38] gray level dependence matrix (GLDM) features and neighboring gray tone difference matrix (NGTDM) features. The wavelet-based features were derived from wavelet decompositions of the original CT images using the "Coiflet 1" wavelet function. Each image was filtered using either a high band-pass filter (H) or low-band pass filter (L) in x, y and z directions, yielding 8 different combinations of decompositions. Finally, a total of 1936 radiomics features were extracted for each patient (pancreas and peripancreatic region). The Z score method was utilized to normalize the values of the radiomics features.

Feature selection

In order to identify robust radiomics features, a three-step procedure was conducted in this study. First, Variables with a correlation coefficient >0.7 were excluded. And the least absolute shrinkage and selection operator (LASSO)[39] is a popular method for selecting the most important variables to include in prediction models. In this study, the LASSO along with the bootstrap method was employed to assess the importance of variables. To perform the LASSO variable selection process, an L1-penalized absolute shrinkage with 10-fold cross-validation was performed. This penalty term encourages sparsity in the resulting model by shrinking the coefficients of irrelevant variables toward zero. Subsequently, univariable and multivariate logistic regression analysis was applied to select the most statistically significant radiomics features related to the AP-AKI.

Radiomicss model development, evaluation and risk stratification

An XGBoost model (denoted by XGBM) was constructed using the optimal features selected on the training set. The Transparent Reporting of a multivariable prediction model for Individual Prognosis or Diagnosis (TRIPOD) guidelines were adhered to improve the reproducibility and rigor of this work.[40] The model's discrimination was assessed with precision-recall (PR) curve[41] and receiver operating characteristic curve (ROC) analysis, and the areas under the curve (AUC) were calculated. The calibration curve was generated to graphically evaluate the relationship between the observed values and the predicted probabilities by risk score. The Brier score was calculated to evaluate the model's calibration. The Brier score is the mean squared error between predicted and observed values.[42] A Brier score of 0 indicates the model's predictions perfectly match the actual values, representing a perfect model. The patients with acute pancreatitis were categorized into high-risk and low-risk groups based on the optimal cutoff value, determined by the Youden index (sensitivity + specificity – 1).

Human reader studies

Since assessing pancreatic inflammation and/or necrosis, as well as peripancreatic inflammation, is crucial for determining the severity of pancreatitis, and widely utilized in clinical practice. We designed the comparative strategies, aiming to compare the XGBM with

contrast-enhanced CT by human readers, to validate whether XGBM could help clinic make more accurate decisions. In addition to that, the human reader with contrast-enhanced CT in predicting AP-AKI was studied. Namely, human reader studies were conducted to compare XGBM radiologists with contrast-enhanced CT in distinguishing those acute pancreatitis patients who will develop acute kidney injury. As such, two pancreatic imaging specialists were employed to estimate the contrast-enhanced CT on D2 and D3. Notably, the human readers were blinded to the ground-truth clinical outcome of the AP patients. Each case was assigned a 10-point score, based on the pancreatic inflammation, along with the assessment of the peripancreatic and extrapancreatic features, as per the previous research conducted by Koenraad.[11] And the AP patients were stratified into low-risk (0–2 points), moderate-risk (4–6 points) and high-risk (8–10 points) groups based on the assigned scores, accordingly.

QUANTIFICATION AND STATISTICAL ANALYSIS

The normality of the data was determined by performing the Kolmogorov-Smirnov Normality Test.[43] For continuous variables, the mean and standard deviation (SD) were calculated if the distribution was normal, or the median and interquartile range (IQR) were calculated if the distribution was not normal. To compare groups of quantitative variables, an unpaired, 2-tailed t-test was used for normal distribution or the Mann-Whitney U test was used when data distribution was skewed. For categorical variables, the results were expressed as whole numbers and percentages (n [%]). To compare groups of qualitative variables, the $\chi 2$ test or Fisher exact test was used. Inter-observer agreement was analyzed using weighted Cohen's Kappa[44] for qualitative variables and Pearson correlation coefficient for quantitative variables. An unpaired t test was used to compare the expression of Serum CRP level between XGBM-positive and XGBM-negative groups.

In this study, statistical significance was defined as $p < 0.05$. All analyses were conducted using the R software, version 4.2.2.